# Online detection of interturn short-circuit fault in induction motor based on 5th harmonic current tracking using Vold-Kalman filter

**Manuel A. Mazzoletti[1], Francisco R. Gentile[2], Pablo D. Donolo[3], Guillermo R. Bossio[3]**
[1]Research and Development Laboratory on Electrical Energy, Faculty of Engineering, UNaM, Misiones, Argentina
[2]Institute of Biomedical Engineering, Faculty of Engineering, University of Buenos Aires, Buenos Aires, Argentina
[3]IITEMA-CONICET, Grupo de Electrónica Aplicada, Universidad Nacional de Río Cuarto, Córdoba, Argentina

## Article Info

## ABSTRACT

In this paper we propose a strategy for real-time detection of interturn short-circuit faults (ISCF) on three-phase induction motor (IM) by using a Vold-Kalman filter (VKF) algorithm. ISCF produce a thermal stress into the stator winding due to large current that flows through the short-circuited turns. Therefore, incipient fault detection is required in order to avoid catastrophic failures such as phase to phase, or phase to ground faults. The strategy is based on an analytical IM model that includes a ISCF fault in any of the phase windings and considering the $h^{-th}$ harmonic in the voltage supply. Based on equivalent electrical circuits with harmonics in sequence components, we propose a strategy for detection of an ISCF on IM by tracking the 5th harmonic current component using a VKF algorithm. The proposed model is experimentally validated using a three-phase IM with modified stator windings to generate ISCF. Also, the IM is fed by a programmable voltage source to synthesize distorted voltage supply with the 5th harmonic. The results demonstrated that the positive-sequence magnitude for the 5th harmonic current component is a good indicator of the fault severity once it exceeds a threshold limit value, even under load variations and unbalanced voltages.

*Corresponding Author:*

Manuel A. Mazzoletti
Research and Development Laboratory on Electrical Energy, Faculty of Engineering, National University of Misiones
National route #12, km 7.5, Misiones, Argentina
Email: armando.mazzoletti@gmail.com

## 1. INTRODUCTION

In a balanced three-phase electrical system, each of harmonic components can be classified as positive, negative or zero sequence [1]. However, several disturbances cause the unbalance of the voltages or currents that originate components in different sequences for the same harmonic order. These disturbances can be attributed to several phenomena such as electrical faults in rotary electric machines or due to external problems arising from the low quality of electrical energy systems, among others. In faulty conditions, the impedances symmetrical become asymmetrical and, consequently, the harmonic components can be used for the detection of the faults [2], [3]. In this context, different methods have been proposed for detection of faults based on signals through the analysis of the components in frequency [4]–[6]. In some industrialized processes, the voltage and current harmonics are generated naturally when the induction machine (IM) is controlled by electric drives such as inverter or soft starters. Based on these characteristics, in [7], the 5th and 7th harmonic

components present different behaviors under high-resistance electrical connections and interturn short-circuit fault (ISCF). However, the effects of external disturbances have not been considered for the robustness analysis of the proposed strategy. It should be noted that the fault detection methods based on the evaluation of the frequency components may present low sensitivity because the effects of a particular fault could be combined with other disturbances such as the unbalance of the voltage supply [8], [9], the high-resistance connections [10], [11] or mechanical faults [12], among others.

In order to attenuates the fault detection errors due to external disturbances, some proposals are based on artificial intelligence (AI) systems such as vector support machines [13], neural networks [14], [15] or rule-based classifier [16]. These methods require an exhaustive training of the learning algorithms for the recognition of fault patterns through tests under different fault severities and operating conditions. In [15] was proposed a faults diagnosis method to detect a instantaneous slip frequency control (ISFC) in stator winding of three-phase high-speed solid rotor IMs. The method is based on the negative sequence of the fundamental current and a fuzzy neural network algorithm. In order to obtain the amplitude and phase angle of negative sequence current a sequence analyzer is used. The performance of the proposed method is evaluated by simulation results for healthy and faulty cases. A study based on short-time Fourier transform for fault classification and identification in voltage source inverter (VSI) switches was proposed in [16]. The method aims to detect the switch faults in VSI based on a rule-based classifier. The performance is validated by categorizing 60 signals for each switch fault. These methods have the advantage of detecting different types of faults. However, the fault diagnosis precision decreases against of limited input data or fault condition not considered in the training stage. In [17], is proposed a frequency response analysis (FRA) technique to detect phase-to-phase faults in three-phase IMs. This same technique is used in [18] to detect ISCF in the stator windings. It should be noted that the FRA response is an offline technique. In other words, FRA technique can be applied during a scheduled maintenance shutdown when the IM is turned off.

To analyze and characterize the faults against the operating conditions variations there are methods based on process model [1]. An accurate analytical model allows solving the problem of generalization of fault classes, reducing errors in fault detection. Most of the analytical models are formulated by means of differential equations of parameters concentrated in $qd0$ reference frame [19]. In this context, the first dynamic models considering a ISCF in the stator windings of the IM were proposed in [20], [21]. The early detection of ISCF is very important to avoid deterioration of the winding insulation that can lead to the most catastrophic faults such as phase-phase or single-phase short circuits or core fault [22]. Due to the fact that ISCF produces slight unbalance in the current, the conventional protections, usually, do not have the necessary capacity for their early detection. However, the fault current flowing between the faulty turns can reach magnitudes several times greater than the nominal current. In [21] was proposed a faulty model for three-phase IM that includes ISCF in any of the phase windings based on [20]. From these reference faulty IM models, various others were proposed in the literature [9], [23]–[26]. A proposed and still current method is based on the analysis of the sequence impedance matrix obtained from the faulty analytical model [27], [28]. In these cases, the detection is carried out by following the terms outside the diagonal of the impedance matrix. It is important to mention that the methods based on the IM model have been proposed considering the effects of faults on the sinusoidally distributed windings, without including harmonics in sequence components.

Different techniques are used to real-time fault diagnosis such as the state observer [21], [29], analysis of the internal signals from the direct field-oriented control [30], monitoring of common-mode impedance [31], Vold-Kalman filter (VKF) algorithm [32]. In previous works, the VKF is used for the estimation of the fundamental component based on an IM fault model [33], [34]. A residual signal is calculated from subtraction between the estimated fundamental component and original signal for ISCF detection. However, the resulting residual signal may also contain the information of other IM faults or the power quality problems. In these previous works, the effects of a ISCF on the harmonic components have not been included.

In this paper we present an online strategy for detection of a ISCF in the windings of the three-phase IM with squirrel cage rotor based on harmonic sequence components analysis of the stator currents. An analytical IM model with ISCF considering the $h$ harmonic in the voltage supply is presented. This extended faulty IM model was proposed in [35] to demonstrate the effects of stator faults on harmonic components. In addition, the IM model allows analyzing the performance of the machine with ISCF under variable operating conditions from the equivalent electrical circuits in sequence components for the steady state. The real-time detection of a ISCF is based on the monitoring and evaluation of the $5^{th}$ harmonic components in the stator currents. Unlike the technique proposed in [35] that uses a classic filter to separate the harmonic components, in this work we propose the tracking of the harmonic components by using a VKF algorithm. The implementation of VKF feature the advantage of eliminating the inherent phase delays introduced by classic filters also minimizes the Gaussian noise and measurement-noise disturbance. The experimental validation of the proposed ISCF detection strategy was carried out using a programmable three-phase voltage source that allows synthesizing different voltage waveforms at the terminals of an IM with modified windings. Finally,

the simulation results and those obtained through experimental tests considering non-sinusoidal voltage waveforms and different load conditions are presented.

The work is organized as follows: the IM dynamic model with ISCF in $qd$ reference frame is presented in section 2. This section also presents the extended faulty IM model for steady state and the highlights feature that can be derived from the proposed extended faulty IM model. The strategy for ISCF detection is developed in section 3. Section 4 presents the simulation results for the IM with ISCF and different load conditions. Finally, section 5 shows the experimental results obtained.

## 2. IM MODEL WITH ISCF

The faulty IM model presented in this section is based on dynamic models proposed in [20], [21]. So, the following simplifying hypotheses were considered for the analytical formulation: IM presents an electromagnetic system with sinusoidal distributions and geometric symmetry; the effects of magnetic saturation are negligible; the iron permeability is considered infinite; losses due to Eddy currents are neglected; zero sequence components are not included due to the no-connect between the center point of the stator windings and the neutral point of the voltage supply; last, the parameters are constant and invariant.

From the previous hypotheses, the IM dynamic model with ISCF in the stationary $qd$ reference frame is given by [21]:

$$v_{qds} = r_s i_{qds} + p\lambda_{qds} - \frac{2}{3}\mu_{qd} r_s i_f \tag{1}$$

$$v_{qdr} = r_r i_{qdr} + p\lambda_{qdr} - \omega_r J\lambda_{qdr} \tag{2}$$

and the fluxes are defined as (3), (4),

$$\lambda_{qds} = L_s i_{qds} + L_m i_{qdr} - \frac{2}{3}\mu_{qd} L_s i_f \tag{3}$$

$$\lambda_{qdr} = L_r i_{qdr} + L_m i_{qds} - \frac{2}{3}\mu_{qd} L_m i_f \tag{4}$$

where the subscripts $s$ and $r$ indicate the magnitudes referred to the stator and the rotor, respectively. $v_{qd} = [v_q\ v_d]^T$, $i_{qd} = [i_q\ i_d]^T$ and $\lambda_{qd} = [\lambda_q\ \lambda_d]^T$ are the voltage, current and magnetic flux vectors, respectively. $L_s = L_{ls} + L_m$ and $L_r = L_{lr} + L_m$, are the inductances of the stator and rotor, respectively. $L_m = \frac{3}{2} L_{ms}$ is the magnetizing inductance and $L_l$ corresponds to the leakage inductance. The fault current is, $i_f$, and $\omega_r$ is the angular rotor speed. $p$ represents the derivative operator and $J = \begin{bmatrix} 0 & -1 \\ 1 & 0 \end{bmatrix}$.

The model for the fault loop formed by the short-circuited turns in the stator winding is expressed as [21],

$$v_{qd}^T\mu_{qd} = \left[\left(1 - \frac{2}{3}\|\mu_{qd}\|\right)\|\mu_{qd}\|\right](r_s + L_{ls}p)i_f + r_f i_f \tag{5}$$

where $\mu_{qd} = \mu [n_q\ n_d]^T \|\mu_{qd}\|$ is the ratio between the faulty and total turns of the phase winding and $\angle\mu_{qd}$ is the ISCF location into stator windings. Thus, according to the faulty phase windings, the $n_q$ and $n_d$ real values can be set as $[1\ 0]^T$ for $a$-phase winding, $[-\frac{1}{2}\ -\frac{\sqrt{3}}{2}]^T$ or $[-\frac{1}{2}\ \frac{\sqrt{3}}{2}]^T$ for $b$- or $c$-phase winding, respectively. For healthy IM condition $\|\mu_{qd}\| = 0$ and the resulting model is the conventional $qd$ dynamic IM model [19].

### 2.1. Extended IM model with ISCF for steady state

The extended faulty IM model is an evolution of the previous dynamic models proposed in [20], [21]. Unlike the others models, the propose faulty model includes harmonics in the voltage supply [35]. Then, by applying non-sinusoidal and unbalanced voltages in sequence components, the arbitrary voltages can be expressed as (6) [19].

$$v_{qdh} = \tilde{V}_{sph}e^{jh\omega_e t} + \tilde{V}_{snh}e^{-jh\omega_e t} \tag{6}$$

Knowing that the electrical angular speed, $\omega_e$, is constant for steady state, the analytical solutions of the currents can be defined according to,

$$i_{qdh} = \check{I}_{sph}e^{jh\omega_e t} + \check{I}_{snh}e^{-jh\omega_e t} \tag{7}$$

where, $\tilde{V}$ and $\tilde{I}$ represent the voltage and current phasors of variable amplitude, the subscripts *sp* and *sn* are the positive- and negative-sequence components, respectively.

The harmonic order is defined by $h = 1, 2, 3, ...n$. Then, from (6) and (7), the extended faulty IM model for the steady state can be expressed as (8)-(11):

$$\tilde{V}_{sph} = (r_s + jh\omega_e L_s)\left(\tilde{I}_{sph} - \frac{1}{3}\mu_{qd}\tilde{I}_f\right) + jh\omega_e L_m \tilde{I}_{rph} \tag{8}$$

$$\tilde{V}_{snh} = (r_s + jh\omega_e L_s)\left(\tilde{I}_{snh} - \frac{1}{3}\mu_{qd}^*\tilde{I}_f\right) + jh\omega_e L_m \tilde{I}_{rnh} \tag{9}$$

$$0 = (r_r A + jh\omega_e L_r)\tilde{I}_{rph} + jh\omega_e L_m\left(\tilde{I}_{sph} - \frac{1}{3}\mu_{qd}\tilde{I}_f\right) \tag{10}$$

$$0 = (r_r B + jh\omega_e L_r)\tilde{I}_{rnh} + jh\omega_e L_m\left(\tilde{I}_{snh} - \frac{1}{3}\mu_{qd}^*\tilde{I}_f\right) \tag{11}$$

where, $A = \frac{h}{h-1+S}$, and $B = \frac{h}{h+1-S}$, with the slip defined by $S = \frac{\omega_e - \omega_r}{\omega_e}$.

Finally, the model for the fault circuit is given by,

$$\mu_{qd}^*\tilde{V}_{sph} + \mu_{qd}\tilde{V}_{snh} = K(r_s + jh\omega_e L_{ls})\tilde{I}_f + r_f\tilde{I}_f \tag{12}$$

where $K = \left(1 - \frac{2}{3}\|\mu_{qd}\|\right)\|\mu_{qd}\|$, $\tilde{I}_f$ is the phasor of the fault current and $r_f$ is the fault resistance.

## 2.2. IM model with ISCF for the 5th harmonic

The proposed extended faulty IM model allows evaluating the effects of a ISCF considering any harmonic sequence components. Particularly, the 5th harmonic features only the negative-sequence component in balanced voltage supply systems. Therefore, from (8) to (12) the IM model with ISCF for $h=5$ can be expressed as:

$$\tilde{V}_{sn5} = (r_s + j5\omega_e L_s)\left(\tilde{I}_{sn5} - \frac{1}{3}\mu_{qd}^*\tilde{I}_f\right) + j5\omega_e L_m \tilde{I}_{rn5} \tag{13}$$

$$0 = \left(r_r\frac{5}{6-S} + j5\omega_e L_r\right)\tilde{I}_{rn5} + j5\omega_e L_m\left(\tilde{I}_{sn5} - \frac{1}{3}\mu_{qd}^*\tilde{I}_f\right) \tag{14}$$

$$\mu_{qd}\tilde{V}_{sn5} = K(r_s + j5\omega_e L_{ls})\tilde{I}_f + r_f\tilde{I}_f \tag{15}$$

The representation of the equivalent circuit for the 5th negative-sequence component it is shown in Figure 1(a). The fault equivalent circuit is shown in Figure 1(b). So, based on the analytical development carried out so far, the following highlights can be derived from the proposed faulty IM model:

− In balanced voltages supply, the 5th harmonic contains only the negative-sequence component, see Figure 1(a). For these conditions, the positive-sequence component is null ($\tilde{V}_{sph} = 0$).
− From (11), the rotor terms, $r_r B$, as a function of slip to $h=5$, show the following characteristics,

$$r_r B = r_r\frac{5}{6-S} \rightarrow \begin{cases} r_r & if \quad S = 1 \\ \frac{5}{6}r_r & if \quad S \rightarrow 0 \end{cases} \tag{16}$$

It can be seen that the equivalent rotor resistance, between locked-rotor ($S=1$) and no-load conditions ($S\rightarrow 0$) presents a limited range of parametric variation for the full IM operating conditions. Thus, based on this highlighted feature, the load variations are attenuated for 5th harmonic.
− Considering the above features, an ISCF in the stator windings originates positive-sequence components and, consequently, the resulting current is a signal proportional to the fault severity whose magnitude is defined as (17),

$$\tilde{I}_{sp5} - \frac{1}{3}\mu_{qd}\tilde{I}_f \tag{17}$$

− Once a ISCF is triggered, from (10), the rotor terms, rr A, as a function of slip to h= 5, show the following characteristics,

$$ r_r A = r_r \frac{5}{4+s} \rightarrow \begin{cases} r_r & if \quad S = 1 \\ \frac{5}{4} r_r & if \quad S \rightarrow 0 \end{cases} \tag{18} $$

Similar to (16), the equivalent rotor resistance presents a limited range for any IM operating condition.
- In faulty IM condition, the amplitude of fault current, $\tilde{I}_f$, is limited only by $rs$, $Lls$, $rf$, and the fault severity, $\|\mu_{qd}\|$.

It should be noted that the total harmonic distortion (THD) is usually least in conventional power electrical systems. However, the harmonic components are generated when IM is controlled by electrical drives [7].
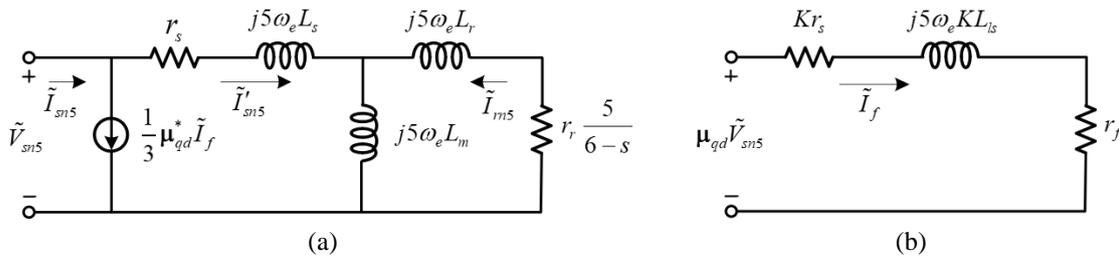


Figure 1. Steady-state IM equivalent electric circuits with an ISCF (a) $5^{th}$ negative-sequence component and (b) fault equivalent electric circuit

## 3. STRATEGY FOR ISCF DETECTION

The ISCF detection is performed by tracking the amplitudes of the positive-sequence current components. The real-time detection strategy is based on two main steps:
- Real-time VKF implementation for $5^{th}$ harmonic tracking.
- Calculation of the sequence current component for ISCF detection.

### 3.1. VKF implementation

The VKF can be characterized in two stages, the prediction and the correction stage. In the first stage, the stochastic variables are calculated based on an analytical model that describes the performance of the stator current components. In this work, the faulty IM model presented in section 2 is used in the prediction stage. In the second stage, the real measured signal is processed for the stochastic variables correction. The VKF algorithm is described in detail in [36]. The discrete state-space model is exposed below:

$$ \begin{bmatrix} x_{1_{0°}} \\ x_{1_{90°}} \\ x_{5_{0°}} \\ x_{5_{90°}} \end{bmatrix}_{k+1} = A_d \begin{bmatrix} x_{1_{0°}} \\ x_{1_{90°}} \\ x_{5_{0°}} \\ x_{5_{90°}} \end{bmatrix}_k + \begin{bmatrix} \gamma_1 \\ \gamma_2 \\ \gamma_3 \\ \gamma_4 \end{bmatrix}_k \tag{19} $$

$$ y_k = C_d \begin{bmatrix} x_{1_{0°}} \\ x_{1_{90°}} \\ x_{5_{0°}} \\ x_{5_{90°}} \end{bmatrix}_k + v_k \tag{20} $$

where, $x_{1_{0°}}$, $x_{5_{0°}}$ and $x_{1_{90°}}$, $x_{5_{90°}}$, are the discrete-time signals of fundamental component and $5^{th}$ harmonic, respectively, in $qd$ stationary reference frame. The $\gamma$ parameter matrix model the Gaussian noise. The output of the model $y_k$ contains the random noise $v_k$ due to measurement noise and the high switching frequency disturbance from electrical motor drivers. Finally, $A_d$ and $C_d$, are defined as,

$$ A_d = \begin{bmatrix} cos(\omega_1 T_s) & sin(\omega_1 T_s) & 0 & 0 \\ -sin(\omega_1 T_s) & cos(\omega_1 T_s) & 0 & 0 \\ 0 & 0 & cos(\omega_5 T_s) & sin(\omega_5 T_s) \\ 0 & 0 & -sin(\omega_5 T_s) & cos(\omega_5 T_s) \end{bmatrix} \quad and \quad C_d = [1 \quad 0 \quad 1 \quad 0], $$

where, $\omega_1 = 2\pi f_1$, with fundamental frequency $f_1 = 50$ Hz and $\omega_5 = 2\pi 5 f_1$.

The VKF algorithm is reduced to the following three main steps:
1) Calculation of $K_k$ gain:

$$K_k = A_d P_k C_d^T (C_d P_k C_d^T + R)^{-1} \tag{21}$$

where, $P_k$ is the covariance matrix of the prediction stage, $R$ is a scalar number of the covariance of the measurement signal.

2) Calculation of estimated states, $\hat{x}_{k+1}$, given by $\hat{x}_k$:

$$\hat{x}_{k+1} = A_d \hat{x}_k + K_k (S_k - C_d \hat{x}_k) \tag{22}$$

where, $S_k$ is the discrete-time signal defined only at discrete-time instants, $k$.

3) Calculation of the covariance matrix for the next iteration:

$$P_{k+1} = A_d P_k A_d^T - K_k C_d P_k A_d^T + Q \tag{23}$$

where, $Q$ is the covariance matrix of the prediction stage.

The Figure 2 shows the results of VKF implementation. Figure 2(a) shows a non-sinusoidal voltage waveform to contain the fundamental frequency component, the 5th harmonic and also the high frequency noise. Once the VKF is applied, the Figure 2(b) shows in detail the correct estimation of the voltage waveform (dashed line) and the elimination of Gaussian noise from the measured signal.
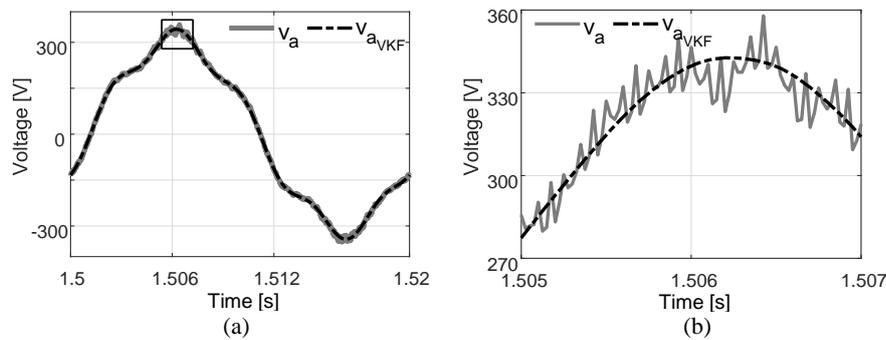


Figure 2. VKF application (a) tracking of the $a$-phase voltage and (b) detail of the filtered signal

## 3.2. Sequence decomposition and magnitude calculation

The sequence decomposition of a voltage or current arbitrary signal can be obtained by (24).

$$\begin{bmatrix} \xi_0 \\ \xi_{sp} \\ \xi_{sn} \end{bmatrix} = T_1 \begin{bmatrix} \xi_a \\ \xi_b \\ \xi_c \end{bmatrix} \tag{24}$$

Where, $\xi_0$, $\xi_{sp}$ and $\xi_{sn}$ are the homopolar, positive- and negative-sequence components signals, respectively. $T_1 = \frac{1}{3} \begin{bmatrix} 1 & 1 & 1 \\ 1 & \sigma & \sigma^2 \\ 1 & \sigma^2 & \sigma \end{bmatrix}$, $\xi_a$, $\xi_b$ and $\xi_c$ are the voltage or current signals of each phase and $\sigma = e^{j120°}$ is a rotation operator. Using trigonometric identities, (24) can be expressed by the sum of two signals as (25).

$$\begin{bmatrix} \xi_0 \\ \xi_{sp} \\ \xi_{sn} \end{bmatrix} = T_\alpha \begin{bmatrix} \xi_{\alpha_a} \\ \xi_{\alpha_b} \\ \xi_{\alpha_c} \end{bmatrix} + T_\beta \begin{bmatrix} \xi_{\beta_a} \\ \xi_{\beta_b} \\ \xi_{\beta_c} \end{bmatrix} \tag{25}$$

Where $\xi_\alpha$ and $\xi_\beta$ are the estimate signals in $\alpha\beta$ reference frame calculated from (22) and $T_\alpha$, $T_\beta$ are defined as,

$$T_\alpha = \frac{1}{3} \begin{bmatrix} 1 & 1 & 1 \\ 1 & \cos\left(\frac{2\pi}{3}\right) & \cos\left(-\frac{2\pi}{3}\right) \\ 1 & \cos\left(-\frac{2\pi}{3}\right) & \cos\left(\frac{2\pi}{3}\right) \end{bmatrix} \quad \text{and} \quad T_\beta = \frac{1}{3} \begin{bmatrix} 1 & 1 & 1 \\ 1 & \sin\left(\frac{2\pi}{3}\right) & \sin\left(-\frac{2\pi}{3}\right) \\ 1 & \sin\left(-\frac{2\pi}{3}\right) & \sin\left(\frac{2\pi}{3}\right) \end{bmatrix}$$

In order to detect an ISCF without errors, a threshold value defined for the healthy IM is required. In this work, the magnitudes of each sequence component are again processed by the VKF in order to calculate the Euclidean norm as (26):

$$\xi_{CS} = \sqrt{\xi_{CS_\alpha}^2 + \xi_{CS_\beta}^2} \tag{26}$$

where $\xi_{CS}$ is the norm of the homopolar, *sp* or *sn* components.

## 4.    PERFORMANCE OF THE PROPOSED STRATEGY IN SIMULATION

In order to evaluate the performance of the proposed ISCF detection strategy, this section shows the simulation results obtained for the faulty IM operating with non-sinusoidal voltage waveforms and different load conditions. The voltage waveforms contain the fundamental frequency and the 5th harmonic. Figure 3 shows the components estimation and the sequence decomposition of the voltage and current signals.

The Figures 3(a) and (b) shows the *a*-phase voltage and the rated current waveform, respectively. Once the VKF is applied, the fundamental frequency, ($v_{a1}$, $i_{a1}$), and the 5th harmonic, ($v_{a5}$, $i_{a5}$), are calculated. Figures 3(c) and (d) shows the sequence decomposition of the fundamental frequency and, Figures 3(e) and (f) for the 5th harmonic. Note the Euclidean norm calculated from (26) that indicates the magnitude of each component. Since the IM is operating at healthy condition and the voltages supply is balanced, the fundamental frequency present only the positive-sequence component, $v_{asp1}$ and $i_{asp1}$. Besides, the 5th harmonic present only the negative-sequence components, $v_{asn5}$ and $i_{asn5}$.
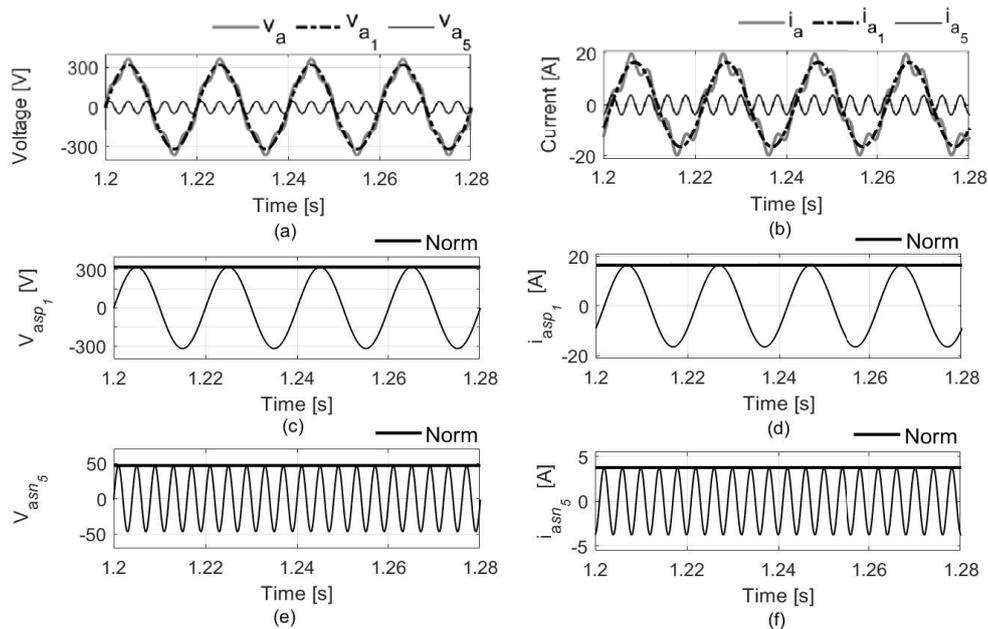


Figure 3. Component estimation and sequence decomposition, (a) *a*-phase voltage, (b) rated current. Positive-sequence component of fundamental frequency (c) voltage and (d) current. Negative-sequence component of 5th harmonic (e) voltage and (f) current

Figure 4 shows the performance of the stator current for the faulty IM. Figure 4(a) shows the resulting current of *a*-phase winding with ISCF triggered at t=1.3 s. Figure 4(b) shows the rated three-phase stator currents. Note that the currents are unbalanced after the ISCF is activated. Figures 4(c) and (d) shows the positive- and negative-sequence component of the fundamental frequency ($i_{asp1}$, $i_{asn1}$), respectively. Figures 4(e) and (f) shows the positive- and negative-sequence component of the 5th harmonic ($i_{asp5}$, $i_{asn5}$), respectively. It is clear that the amplitude of the $i_{asp5}$ component increases and remains at a constant value at the time the ISCF is triggered.

The Figure 5(a) shows the faulty IM operating with different load conditions. Before t=1.3 s the IM is at no-load, between 1.3 s and 1.6 s at 50% of full-load, then 1.6 s at full-load condition. In the same way as the previous case, the ISCF is triggered at t=1.3 s. Figure 5(a) shows the *a*-phase current and Figure 5(b) shows

the performance of three-phase currents for the three load conditions mentioned above. Figures 5(c) and (d) shows the $i_{asp1}$ and $i_{asn1}$, respectively. Note that both components having notable variations against the load changes. On the other hand, Figures 5(e) and (f) shows the $i_{asp5}$ and $i_{asn5}$, respectively. Similar to Figure 4(e), the $i_{asp5}$ component increases at the time the ISCF is triggered. In this case, the load variations cause a minimal transient magnitude change on the component but hold on its value at full operating range. In the last Figure 5(f), the negative-sequence component no indicates significant magnitude changes.
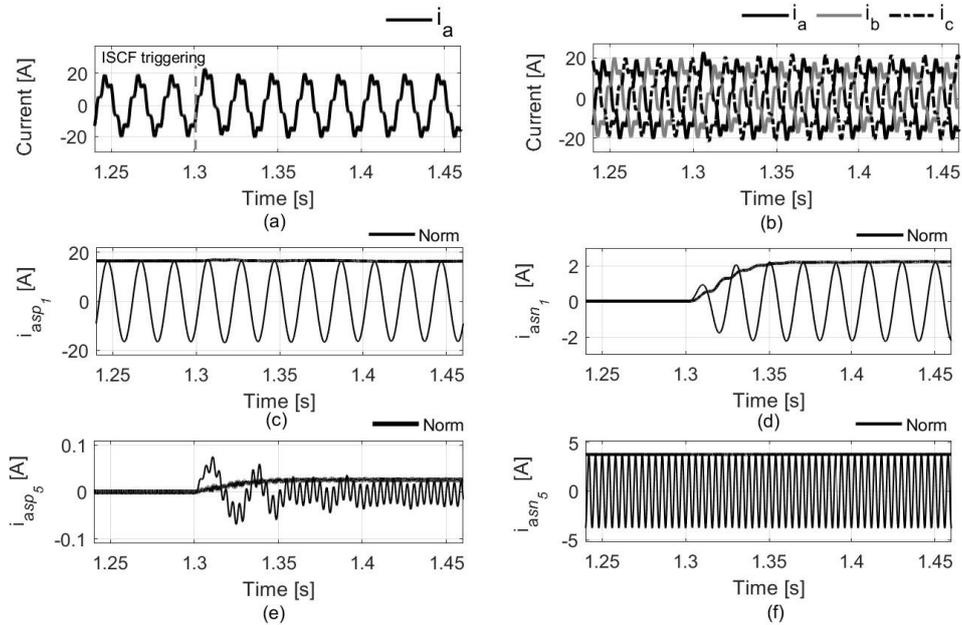


Figure 4. Faulty IM operating at full-load, (a) *a*-phase current with ISCF, (b) three-phase current. Fundamental frequency (c) positive-sequence, and (d) negative-sequence component. 5th harmonic, (e) positive-sequence, and (f) negative-sequence component
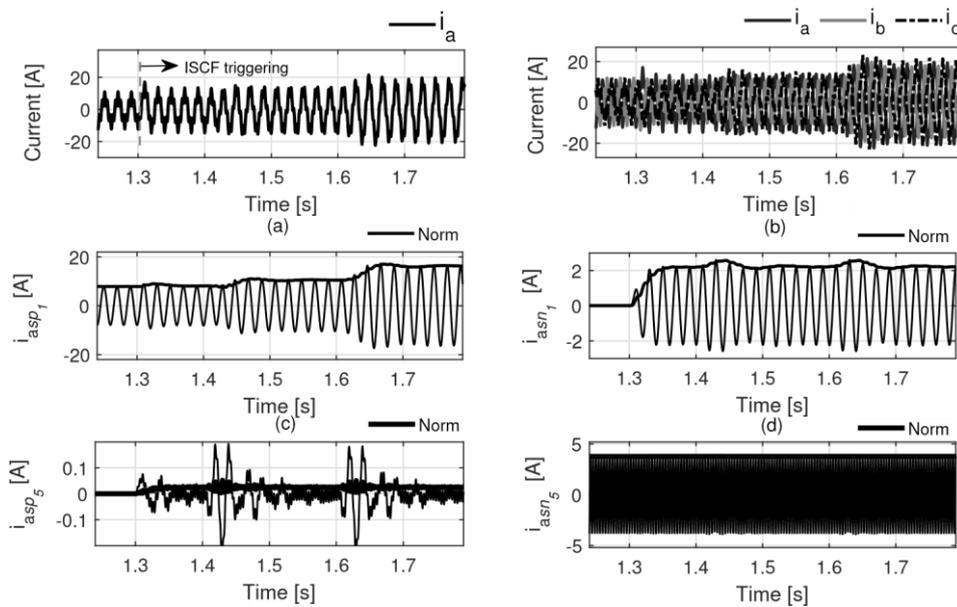


Figure 5. Faulty IM operating under different load conditions, (a) *a*-phase current with ISCF, (b) three-phase current. Fundamental frequency (c) positive-sequence, and (d) negative-sequence component. 5th harmonic (e) positive-sequence, and (f) negative-sequence component

## 5.    EXPERIMENTAL VALIDATION

The experimental laboratory tests were carried out with a programmable voltage source and a three-phase IM with modified stator windings. The voltage source used allows us to synthesize different waveforms of variable amplitude and frequency to generate harmonic distortion controllable. The source consists of an autotransformer that allows adjusting the input voltage level, then a three-phase rectifier and an inverter controlled through a digital signal processor (DSP). The fundamental component and the order of the harmonics to feed the motor are selected by the user from a personal computer (PC). To carry out the tests under load, the shaft of the three-phase IM under test is mechanically coupled to the shaft of a secondary machine driven by means of a commercial drive with torque control. The modified stator windings of the IM present additional outputs to access the 3rd, 5th and 10th turns which makes it possible to generate ISCF of variable severity, between 2% and 7% of total turns of the one-phase winding. Besides, an external resistance of $r_f=149$ $m\Omega$ was inserted between the faulty turns in order to protect the stator winding against high fault currents, similarity to other proposals [21], [35]. Finally, the electrical variables were acquired by using a four-channel oscillographic recorder with a fixed sampling frequency of 40 kS/s. The acquired data was processed on a PC. Table 1 shows the parameters of the prototype IM.

Table 1. Three-phase IM parameters

| Characteristic | Magnitude | Units |
|---|---|---|
| Rated voltage | 380 | V |
| Rated current | 11.7 | A |
| Rated speed | 1470 | rpm |
| Number of Pole Pairs | 2 | − |
| rs | 0.9 | Ω |
| rr | 0.4 | Ω |
| Lls | 4.0 | mH |
| Llr | 4.0 | mH |
| Lm | 125 | mH |

The Figures 6(a) and (b) shows the three-phase voltage supply and the rated current waveforms measured, respectively. The programmable voltage source was configured to introduce a THD=15%. Figure 6(c) shows the $a$-phase voltage and the estimated components, $v_{a1}$ and $v_{a5}$. Similarly, Figure 6(d) shows the $a$-phase current waveform and the estimated components, $i_{a1}$ and $i_{a5}$.
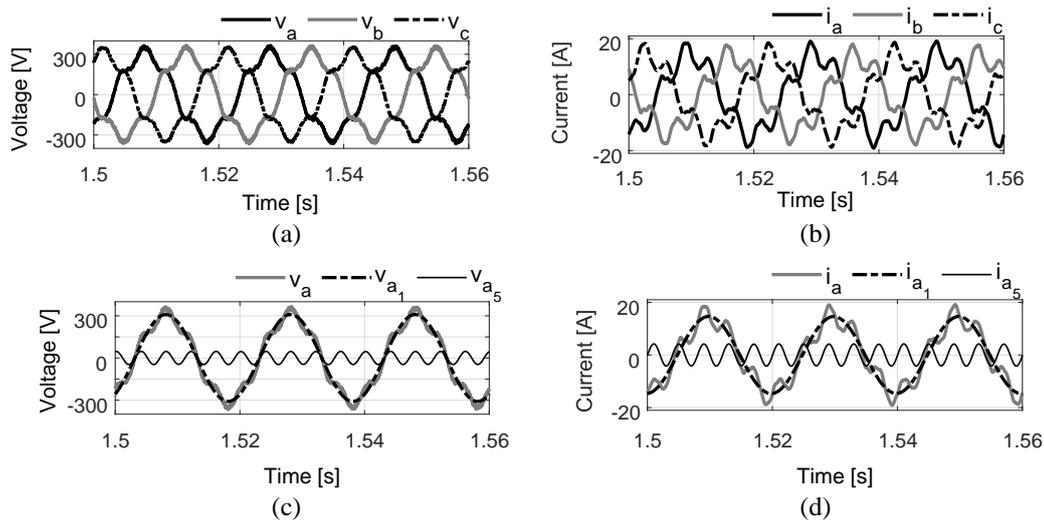


Figure 6. Experimental signals measured on healthy IM operation, (a) voltage supply with THD=15%, (b) three-phase stator current, (c) $a$-phase voltage, and (d) current components estimation

In the practice, the power supply is not fully balanced and the healthy IM may have inherent asymmetries. Because of these disturbances, the current signals may have positive- and negative-sequence components for the same harmonic order, as shown in Figure 7. Figures 7(a) and (b) shows the positive- and negative-sequence component for the fundamental frequency, respectively. On the other hand, Figures 7(c) and

(b) shows the positive- and negative-sequence component for 5$^{th}$ harmonic, respectively. Both, $i_{asn1}$ and $i_{asp5}$ components, are generated due to the aforementioned disturbances. In this case, a threshold limit value must be defined to indicate the healthy operating condition of the IM, as shown in Figure 7(d). In another case, stator fault condition occurs when the magnitude exceeds the preset threshold limit.
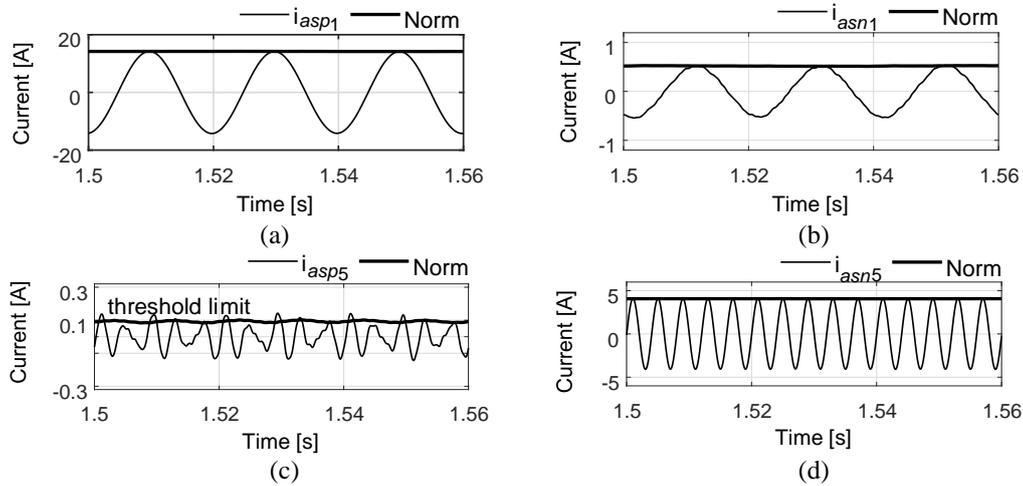


Figure 7. Experimental current measured for healthy IM operation, (a) positive-sequence and (b) negative-sequence of fundamental frequency, (c) positive-sequence, and (d) negative-sequence of 5$^{th}$ harmonic

Finally, the experimental results for the faulty IM under different loading conditions is shown in Figure 8. Both, Figures 8(a) and (b) shows the positive-sequence component performance for 5$^{th}$ harmonic, respectively. Figure 8(a) shows the $i_{asp5}$ magnitudes for IM with 5 (3.5%) and 10 (7%) shorted turns in the $a$-phase winding at 50% of full-load. Note that the magnitude exceeds the threshold limit value only for a fault severity of 7%. On the other hand, in the Figure 8(b) it can be seen that both magnitudes increase at the full-load condition. Unlike the previous load condition, notice that the component magnitude for a 3.5% fault severity is equal to the threshold limit. Therefore, the IM operating at full-load improves the sensitivity in ISCF detection.
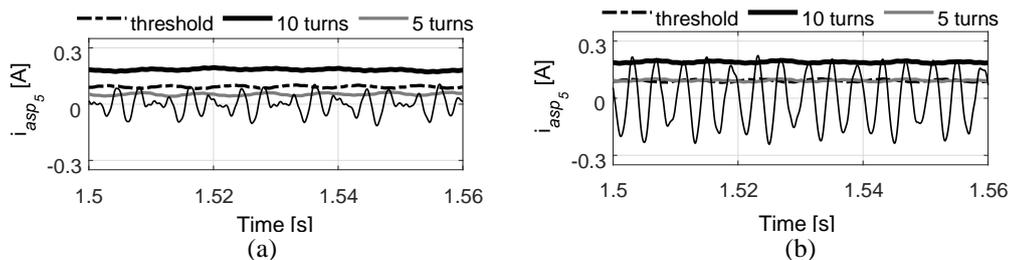


Figure 8. Evolution of positive-sequence component of 5$^{th}$ harmonic for different ISCF severities, (a) 50% of full-load and (b) full-load condition

## 6.    CONCLUSION

In this paper, a strategy for detection of ISCF on three-phase IM with squirrel cage rotor was presented. An analytical IM model with ISCF was proposed considering the $h^{-th}$ harmonic in the voltage supply. The developed model allowed us to analyze the effects of an ISCF on the IM windings from the equivalent electrical circuits in sequence components for the steady state. The proposed strategy showed that an ISCF can be detected by tracking the positive-sequence current component for 5$^{th}$ harmonic. To achieve this goal, a VKF algorithm is used to, first, estimate the fundamental frequency and the 5$^{th}$ harmonic in the voltage and current signals and, second, calculate the Euclidean norm for each sequence component. The simulation results demonstrated that the magnitude of the positive sequence current component for 5$^{th}$ harmonic increases at the time the ISCF is triggered. Also, its showed that the load variations cause changes of transient amplitude on

the component but the magnitude hold on its value for the same fault severity. In order to synthesize non-sinusoidal voltages waveforms, a programmable voltage source was used for carry out laboratory tests. In the practice, the inherent asymmetries of IM or external disturbances may produce nonzero positive-sequence components and, therefore, a threshold limit value was established for the healthy IM in order to avoid false alarms. The experimental results demonstrated that the positive-sequence current magnitude for the 5th harmonic is a good indicator of the fault severity, even under different load conditions. However, for IM at 50% of full-load make it difficult to detect low fault severity due to the magnitude of the positive-sequence current does not exceed the threshold limit value. In summary, the proposed strategy demonstrated that a progressive increase of the positive-sequence current component for the 5th harmonic allows the detection of an ISCF on the IM stator windings.

## ACKNOWLEDGEMENTS

## REFERENCES

[1] R. Isermann, *Fault-diagnosis applications: model-based condition monitoring actuators, drives, machinery, plants, sensors, and fault-tolerant systems*. Berlin, Heidelberg: Springer Berlin Heidelberg, 2011, doi: 10.1007/978-3-642-12767-0.

[2] S. Nandi, H. A. Toliyat, and X. Li, "Condition monitoring and fault diagnosis of electrical motors—a review," *IEEE Transactions on Energy Conversion*, vol. 20, no. 4, pp. 719–729, Dec. 2005, doi: 10.1109/TEC.2005.847955.

[3] C. J. Verucchi and G. G. Acosta, "Fault detection and diagnosis techniques in induction electrical machines," *IEEE Latin America Transactions*, vol. 5, no. 1, pp. 41–49, Mar. 2007, doi: 10.1109/T-LA.2007.4444532.

[4] S. Karmakar, S. Chattopadhyay, M. Mitra, and S. Sengupta, *Induction motor fault diagnosis. Approach through current signature analysis*. Singapore: Springer Singapore, 2016, doi: 10.1007/978-981-10-0624-1.

[5] M. A. AL-Yoonus and O. S. Al-deen Alyozbaky, "Detection of internal and external faults of single-phase induction motor using current signature," *International Journal of Electrical and Computer Engineering (IJECE)*, vol. 11, no. 4, pp. 2830–2841, Aug. 2021, doi: 10.11591/ijece.v11i4.pp2830-2841.

[6] O. Alshorman and A. Alshorman, "A review of intelligent methods for condition monitoring and fault diagnosis of stator and rotor faults of induction machines," *International Journal of Electrical and Computer Engineering (IJECE)*, vol. 11, no. 4, pp. 2820–2829, Aug. 2021, doi: 10.11591/ijece.v11i4.pp2820-2829.

[7] F. Briz, M. W. Degner, J. M. Guerrero, and P. Garcia, "Stator windings fault diagnostics of induction machines operated from inverters and soft-starters using high-frequency negative-sequence currents," *IEEE Transactions on Industry Applications*, vol. 45, no. 5, pp. 1637–1646, 2009, doi: 10.1109/TIA.2009.2027198.

[8] S. Das, P. Purkait, and S. Chakravorti, "Separating induction motor current Signature for stator winding faults from that due to supply voltage unbalances," in *2012 1st International Conference on Power and Energy in NERIST (ICPEN)*, Dec. 2012, pp. 1–6, doi: 10.1109/ICPEN.2012.6492315.

[9] V. Nguyen *et al.*, "A method for incipient interturn fault detection and severity estimation of induction motors under inherent asymmetry and voltage imbalance," *IEEE Transactions on Transportation Electrification*, vol. 3, no. 3, pp. 703–715, Sep. 2017, doi: 10.1109/TTE.2017.2726351.

[10] P. M. de la Barrera, G. R. Bossio, and R. Leidhold, "Online voltage sensorless high-resistance connection diagnosis in induction motor drives," *IEEE Transactions on Industrial Electronics*, vol. 62, no. 7, pp. 4374–4384, Jul. 2015, doi: 10.1109/TIE.2014.2385038.

[11] J. Zhang, J. Hang, S. Ding, and M. Cheng, "Online diagnosis and localization of high-resistance connection in PMSM With improved fault indicator," *IEEE Transactions on Power Electronics*, vol. 32, no. 5, pp. 3585–3594, May 2017, doi: 10.1109/TPEL.2016.2587670.

[12] S. Sridhar, K. U. Rao, K. S. Harish, and R. Umesh, "Condition monitoring of induction motor using negative sequence component and THD of the stator current," in *2016 IEEE 7th Power India International Conference (PIICON)*, Nov. 2016, pp. 1–6, doi: 10.1109/POWERI.2016.8077416.

[13] M. Z. Ali, M. N. S. K. Shabbir, S. M. K. Zaman, and X. Liang, "Machine learning based fault diagnosis for single-and multi-faults for induction motors fed by variable frequency drives," in *2019 IEEE Industry Applications Society Annual Meeting*, Sep. 2019, pp. 1–14, doi: 10.1109/IAS.2019.8912395.

[14] G. H. Bazan, P. R. Scalassara, W. Endo, A. Goedtel, R. H. C. Palacios, and W. F. Godoy, "Stator short-circuit diagnosis in induction motors using mutual information and intelligent systems," *IEEE Transactions on Industrial Electronics*, vol. 66, no. 4, pp. 3237–3246, Apr. 2019, doi: 10.1109/TIE.2018.2840983.

[15] A. T. Radhi and W. H. Zayer, "Faults diagnosis in stator windings of high speed solid rotor induction motors using fuzzy neural network," *International Journal of Power Electronics and Drive Systems (IJPEDS)*, vol. 12, no. 1, pp. 597–611, Mar. 2021, doi: 10.11591/ijpeds.v12.i1.pp597-611.

[16] M. Manap, S. Nikolovski, A. Skamyin, R. Karim, T. Sutikno, and M. H. Jopri, "An analysis of voltage source inverter switches fault classification using short time fourier transform," *International Journal of Power Electronics and Drive Systems (IJPEDS)*, vol. 12, no. 4, pp. 2209–2220, Dec. 2021, doi: 10.11591/ijpeds.v12.i4.pp2209-2220.

[17] A. A. Alawady, M. F. M. Yousof, N. Azis, and M. A. Talib, "Phase to phase fault detection of 3-phase induction motor using FRA technique," *International Journal of Power Electronics and Drive Systems (IJPEDS)*, vol. 11, no. 3, pp. 1241–1248, Sep. 2020, doi: 10.11591/ijpeds.v11.i3.pp1241-1248.

[18] A. A. Alawady, M. F. M. Yousof, N. Azis, and M. A. Talib, "Frequency response analysis technique for induction motor short circuit faults detection," *International Journal of Power Electronics and Drive Systems (IJPEDS)*, vol. 11, no. 3, pp. 1653–1659, Sep. 2020, doi: 10.11591/ijpeds.v11.i3.pp1653-1659.

[19] P. C. Krause, O. Wasynczuk, and S. D. Sudhoff, *Analysis of electric machinery and drive systems*. Wiley-IEEE Press, 2002.

[20] R. M. Tallam, T. G. Habetler, and R. G. Harley, "Transient model for induction machines with stator winding turn faults," *IEEE Transactions on Industry Applications*, vol. 38, no. 3, pp. 632–637, May 2002, doi: 10.1109/TIA.2002.1003411.

[21] C. H. De Angelo, G. R. Bossio, S. J. Giaccone, M. I. Valla, J. A. Solsona, and G. O. Garcia, "Online model-based stator-fault detection and identification in induction motors," *IEEE Transactions on Industrial Electronics*, vol. 56, no. 11, pp. 4671–4680, Nov. 2009, doi: 10.1109/TIE.2009.2012468.

[22] A. Bellini, F. Filippetti, C. Tassoni, and G.-A. Capolino, "Advances in diagnostic techniques for induction machines," *IEEE Transactions on Industrial Electronics*, vol. 55, no. 12, pp. 4109–4126, Dec. 2008, doi: 10.1109/TIE.2008.2007527.

[23] M. Eftekhari, M. Moallem, S. Sadri, and M.-F. Hsieh, "Online detection of induction motor's stator winding short-circuit faults," *IEEE Systems Journal*, vol. 8, no. 4, pp. 1272–1282, Dec. 2014, doi: 10.1109/JSYST.2013.2288172.

[24] D. C. Patel and M. C. Chandorkar, "Modeling and analysis of stator interturn fault location effects on induction machines," *IEEE Transactions on Industrial Electronics*, vol. 61, no. 9, pp. 4552–4564, Sep. 2014, doi: 10.1109/TIE.2013.2288191.

[25] B.-G. Gu, "Offline interturn fault diagnosis method for induction motors by impedance analysis," *IEEE Transactions on Industrial Electronics*, vol. 65, no. 7, pp. 5913–5920, Jul. 2018, doi: 10.1109/TIE.2017.2782200.

[26] F. Babaa and O. Bennis, "An accurate inter-turn short circuit faults model dedicated to induction motors," *International Journal of Electrical and Computer Engineering (IJECE)*, vol. 11, no. 1, pp. 9–16, Feb. 2021, doi: 10.11591/ijece.v11i1.pp9-16.

[27] Sang Bin Lee, R. M. Tallam, and T. G. Habetler, "A robust, on-line turn-fault detection technique for induction machines based on monitoring the sequence component impedance matrix," *IEEE Transactions on Power Electronics*, vol. 18, no. 3, pp. 865–872, May 2003, doi: 10.1109/TPEL.2003.810848.

[28] A. Berzoy, H. H. Eldeeb, and O. A. Mohammed, "On-line detection of stator faults in DTC-driven IM using SC impedance matrix off-diagonal term," *IEEE Transactions on Industry Applications*, vol. 55, no. 6, pp. 5906–5915, Nov. 2019, doi: 10.1109/TIA.2019.2940871.

[29] K. El Merraoui, A. Ferdjouni, and M. Bounekhla, "Real time observer-based stator fault diagnosis for IM," *International Journal of Electrical and Computer Engineering (IJECE)*, vol. 10, no. 1, pp. 210–222, Feb. 2020, doi: 10.11591/ijece.v10i1.pp210-222.

[30] M. Wolkiewicz, G. Tarchala, T. Orlowska-Kowalska, and C. T. Kowalski, "Online stator interturn short circuits monitoring in the DFOC induction-motor drive," *IEEE Transactions on Industrial Electronics*, vol. 63, no. 4, pp. 2517–2528, Apr. 2016, doi: 10.1109/TIE.2016.2520902.

[31] Z. Zhao, F. Fan, W. Wang, Y. Liu, and K. Y. See, "Detection of stator interturn short-circuit faults in inverter-fed induction motors by online common-mode impedance monitoring," *IEEE Transactions on Instrumentation and Measurement*, vol. 70, pp. 1–10, 2021, doi: 10.1109/TIM.2021.3066193.

[32] H. Jafari, J. Poshtan, and S. Shamaghdari, "Stochastic event-triggered fault detection and isolation based on kalman filter," *IEEE Transactions on Cybernetics*, vol. 52, no. 11, pp. 12329–12339, Nov. 2022, doi: 10.1109/TCYB.2021.3107495.

[33] N. R. B. Hatem, M. Mostefai, and O. E. K. Aktouf, "Extended Kalman observer based sensor fault detection," *International Journal of Electrical and Computer Engineering (IJECE)*, vol. 9, no. 3, pp. 1546–1552, Jun. 2019, doi: 10.11591/ijece.v9i3.pp1546-1552.

[34] A. Namdar, H. Samet, M. Allahbakhshi, M. Tajdinian, and T. Ghanbari, "A robust stator inter-turn fault detection in induction motor utilizing Kalman filter-based algorithm," *Measurement*, vol. 187, Jan. 2022, doi: 10.1016/j.measurement.2021.110181.

[35] M. A. Mazzoletti, P. D. Donolo, C. M. Pezzani, M. O. Oliveira, G. R. Bossio, and C. H. De Angelo, "Stator faults detection on induction motors using harmonic sequence current components analysis," *IEEE Latin America Transactions*, vol. 19, no. 5, pp. 726–734, May 2021, doi: 10.1109/TLA.2021.9448286.

[36] R. Cardoso, R. F. de Camargo, H. Pinheiro, and H. A. Grundling, "Kalman filter based synchronization methods," in *37th IEEE Power Electronics Specialists Conference*, 2006, pp. 1–7, doi: 10.1109/PESC.2006.1712058.

## BIOGRAPHIES OF AUTHORS

**Manuel A. Mazzoletti** 🆔 📇 SC 🔗 is graduate research that received his Electronic Engineering degree from the Universidad Nacional de Misiones, Argentina (UNaM), in 2006, and the Doctor of Engineering degree from the Universidad Nacional de Río Cuarto (UNRC), Argentina, in 2017. From 2012 to 2017, he was with the Grupo de Electronica Aplicada (GEA), UNRC. Since 2017, he has been with the Laboratorio de Investigacion y Desarrollo en Energía Electrica (LIDEE), UNaM. He is currently Professor Assistant at UNaM and also with Consejo Nacional de Investigaciones Científicas y Tecnicas (CONICET), Argentina. His research interests include fault diagnosis on electric machines, ac motor drives, energy efficiency in electrical systems and renewable energy generation. He can be contacted at armando.mazzoletti@fio.unam.edu.ar.

**Francisco R. Gentile** 🆔 📇 SC 🔗 received the B.S. degree in Electronic Engineering from the Universidad Nacional de Misiones, (UNaM), Argentina, in 2004 and M.Sc. in Electronic Engineering from the UNAM and simultaneously Electrical Engineering from the Federal University of Santa Maria (UFSM), RS, Brazil, in 2020. Actually, is performing doctorade focused in the artificial intelligence area. Gentile's research interests include signal processing, power electronics, digital control, adaptive control, computational intelligence, internet of everything, computer vision and mobile robotics. He can be contacted at fgentile.ext@fi.uba.ar.

**Pablo D. Donolo** received his Electrical Engineering degree (2006), his MS degree in Engineering Sciences (2013), and his Doctorate in Engineering Sciences (2014) from Universidad Nacional de Río Cuarto, Argentina. In 2005, he joined the Grupo de Electronica Aplicada, Universidad Nacional de Río Cuarto. He is currently Professor Assistant at Universidad Nacional de Río Cuarto and Assistant Researcher at Consejo Nacional de Investigaciones Cient´ıficas y Tecnicas (CONICET), Argentina. His research interests include energy efficiency, power quality and fault diagnosis on electric machines. He can be contacted at pdonolo@ing.unrc.edu.ar.

**Guillermo R. Bossio** received his Electrical Engineering degree from Universidad Nacional de Río Cuarto (UNRC), Argentina, in 1999, and his Doctorate of Engineering degree from the Universidad Nacional de La Plata, Argentina, in 2004. Since 1994, he has been with the Grupo de Electronica Aplicada (GEA), Facultad de Ingeniería, UNRC. He is also currently with Consejo Nacional de Investigaciones Científicas y Técnicas (CONICET), Argentina. His research interests include fault diagnosis on electric machines, AC motor drives, electric vehicles, and renewable energy generation. He can be contacted at gbossio@ing.unrc.edu.ar.